Journal of Nuclear Medicine, published on November 19, 2015 as doi:10.2967/jnumed.115.161653

PET-Based Human Dosimetry of the Dimeric $\alpha_v\beta_3$ Integrin Ligand ^{68}Ga-DOTA-E-[c(RGDfK)]$_2$, a Potential Tracer for Imaging Tumor Angiogenesis

Short running title: Human dosimetry of 68GaDOTA-E[c(RGDfK)]2

Victoria López-Rodríguez[1], Carlos Galindo-Sarco[2], Francisco O. García-Pérez[3], Guillermina Ferro-Flores[4], Oscar Arrieta[5], Miguel A. Ávila-Rodríguez[1]

[1]Unidad Radiofarmacia-Ciclotrón, Facultad de Medicina, Universidad Nacional Autónoma de México, México, D.F., 04510, MEXICO, [2]Departamento de Radiología, Instituto Nacional de Cancerología, México, D.F., 14080, MEXICO, [3]Departamento de Medicina Nuclear, Instituto Nacional de Cancerología, México, D.F., 14080, MEXICO, [4]Gerencia de Aplicaciones Nucleares en la Salud, Instituto Nacional de Investigaciones Nucleares, Ocoyoacac, Edo. de México, 52750, MEXICO, [5]Departamento de Oncología Médica, Instituto Nacional de Cancerología, México, D.F., 14080, MEXICO

Corresponding author	**First author**
Miguel A. Ávila-Rodríguez Unidad Radiofarmacia-Ciclotrón División de Investigación Facultad de Medicina, UNAM Torre de Investigación, P.B. Ciudad Universitaria, Circ. Exterior México, D.F., 04510, MEXICO Tel: +52 55 56232288 Fax: +52 55 56232115 Email: avilarod@uwalumni.com	Victoria López-Rodríguez Unidad Radiofarmacia-Ciclotrón División de Investigación Facultad de Medicina, UNAM Torre de Investigación, P.B. Ciudad Universitaria, Circ. Exterior México, D.F., 04510, MEXICO Tel: +52 55 56228222 Ext 45044 Fax: +52 55 56232115 Email: jaelis28@gmail.com

ABSTRACT

Peptides containing the RGD sequence have high affinity for $\alpha_v\beta_3$ integrin receptors overexpressed in tumor cells. The objective of this research was to determine the biodistribution and estimate the radiation dose from ^{68}Ga-DOTA-E-[c(RGDfK)]$_2$ using whole-body (WB) PET scans in humans. **Methods:** Five healthy volunteers (2 women, 3 men, 37.2±15.6 y, 28-65 y, 79.2±21.0 Kg, 64-115 Kg) were included. After I.V. injection of the tracer (198.3 ± 3.3 MBq), 3 successive WB (vertex to mid-thigh) PET/CT scans at 3 time points (30, 60 and 120 min) were obtained on a Siemens Biograph 16 PET/CT. Subjects did not void the bladder until the entire series of images was completed. Low-dose CT scan without contrast was used for anatomic localization and attenuation correction. OLINDA/EXM software was used to calculate human radiation doses using the reference adult model. **Results:** The highest uptake was in the urinary bladder, followed by the liver, kidneys, and spleen, in descending order. The critical organ was urinary bladder wall. The mean effective doses (all subjects, men and women) were 34.1±4.9 μSv/MBq, 31.0±2.4 μSv/MBq, and 20.9±5.2 μSv/MBq for the no bladder voiding, 2.5- and 1-h bladder-voiding models, respectively. **Conclusion:** Of particular interest in this research was the visualization of the choroid plexus and ventricular system, not previously reported in humans for any RGD radiopeptide. Measured absorbed doses and effective doses are comparable to other previously reported RGD-based radiopharmaceuticals labeled with ^{68}Ga and ^{18}F. Therefore, ^{68}Ga-DOTA-E-[c(RGDfK)]$_2$ can safely be used for imaging integrin $\alpha_V\beta_3$ expression.

Key Words: ^{68}Ga-DOTA-E-[c(RGDfK)]$_2$; $\alpha_V\beta_3$ integrin receptors; angiogenesis; human dosimetry; dimeric RGD peptides

INTRODUCTION

The last few years have witnessed the development of a virtual revolution in Positron Emission Tomography (PET) molecular imaging and radiolabeled receptor-binding peptides are emerging as powerful tools for imaging and therapy applications of tumors expressing peptide binding receptors (1-3). Somatostatin analogues have been in use the longest and have led to the accumulation of a vast amount of data and have proven useful for the management of patients suffering from neuroendocrine tumors (4-8). Several other peptide receptor-binding compounds have been synthesized within the past few years and are currently in various research stages: *in vitro, in vivo*, and pre-clinical studies, but they have not yet been approved for clinical use (9-11). These new and rapidly expanding peptide-based radiopharmaceuticals deserve close attention.

It has been shown that peptides based on the Arg-Gly-Asp (RGD) amino acid sequence have a high affinity and selectivity for $\alpha_v\beta_3$ integrin receptors (12). The $\alpha_v\beta_3$ integrins are transmembrane proteins which are preferentially expressed on proliferating endothelial cells whereas they are absent on quiescent endothelial cells (13). Integrins are over expressed on newly formed blood vessels of actively growing tumors, and are therefore potential targets for receptor-mediated tumor imaging and therapy when labeled with the proper radionuclide. Angiogenesis, the formation of new blood vessels from existing ones, is an essential process in solid tumors growing beyond 2 to 3 mm^3, since diffusion is no longer sufficient to supply the tissue with oxygen and nutrients. Integrins $\alpha_v\beta_3$ have been shown to play an important role in a series of pathological processes including angiogenesis and tumor cell metastasis (2,13-18). Given the high affinity of RGD-based peptides for $\alpha_v\beta_3$ integrin receptors, a variety of cyclic RGD peptide conjugates have been used to target tumors over-expressing these receptors (9-12,14-16,19,20). However, it has been demonstrated that the dimeric conjugate is more suitable, for both imaging and therapeutic applications, than the monomeric conjugate. Li et al. showed that the dimeric and monomeric peptide had similar tumor-to-kidney ratios but the dimer had higher

tumor uptake and a prolonged retention time, making it more suitable than the monomer (21).

The choice of a radionuclide for PET-based molecular imaging applications depends on many parameters including its physical half-life, decay profile, chemistry, *in vivo* kinetics and also important is the availability/cost. In this regard, the availability of the ^{68}Ge/^{68}Ga generator is ideally suited for the demand of ^{68}Ga for clinical applications in PET centers that lack in-site cyclotrons (22-25). ^{68}Ga is a positron emitter with 68 min half-life and good characteristics for PET imaging (89% β^+, $E_{\beta max}$ 1.899 MeV). Additionally, the long half-life of ^{68}Ge (271 days) is attractive to operate the generator over a long period of time on a cost effective manner.

Recently, a number of publications have reported on various radiolabeled RGD containing peptides with high affinity and selectivity for $\alpha_V\beta_3$ integrin receptors both *in vitro* and *in vivo* in animal models (10,14-16). Additionally, detailed biodistribution and measured radiation dosimetry in humans have been reported for ^{18}F-GalactoRGD (26), ^{18}F-RGD-K5 (27*27*), and ^{68}Ga-NOTA-RGD (28). However, despite the proven higher affinity of RGD-dimeric conjugates for $\alpha_V\beta_3$ integrin receptors (17-20,29,30) and that ^{99m}Tc-RGD-dimeric derivatives have been evaluated in humans (**Error! Reference source not found.**,32), only monomeric peptides have been used with PET radionuclides.

The aim of this research was to measure the human radiation dosimetry of ^{68}Ga labeled DOTA-conjugated dimeric RGD peptide, E-[c(RGDfK)]$_2$, using biodistribution data obtained from whole body PET/CT scans in healthy volunteers.

MATERIALS AND METHODS

RADIOPHARMACEUTICAL PREPARATION

Ultrapure (>99.999% trace metal basis) hydrochloric acid (HCl) and sodium acetate (NaOAc) were purchase from Sigma-Aldrich (St. Louis, MO, USA). Cyclo(L-arginylglycyl-L-α-

aspartyl-D-phenylalanyl-L-lysyl), 5,5'-[N-[[4,7,10-tris(carboxymethyl)-1,4,7,10-tetraazacyclododec-1-yl]acetyl]-L-glutamoyl]bis- (DOTA-E-[c(RGDfK)]$_2$) was obtained from ABX Advanced Biomedical Compounds (Radenberg, Germany). Gallium-68 was obtained from an ITG ^{68}Ge/^{68}Ga generator (Isotope Technologies Garching GmbH, Germany). Generator was eluted with 4 ml of 0.05M HCl and labeling was carried out using a fractionation elution method. The first and last fractions of $^{68}GaCl_3$ (1.0 and 1.7 ml, respectively) were discharged, and only the second fraction (1.3 ml), containing approximately 80% of the activity, was used for labeling. Briefly, in a 1.5 ml Eppendorf tube containing 50 µg of DOTA-E-[c(RGDfK)]$_2$ and 165 µl of 0.5M NaOAc were added 1.3 ml of freshly eluted $^{68}GaCl_3$ (~740 MBq). The reaction mixture (pH ~4.0) was at 95 °C in a compact thermomixer (Eppendorf, USA) at 300 rpm. The final product was diluted with 4 ml of physiological saline solution and sterilized by passing it through a 0.22 µm syringe filter (Millex-GV). When needed, purification of the final product was performed by SPE using Oasis HLB cartridges (Waters). The structural formula of ^{68}Ga-DOTA-E-[c(RGDfK)]$_2$ is shown in Fig. 1.

The radiochemical purity (RCP) of ^{68}Ga-DOTA-E-[c(RGDfK)]$_2$ was determined by analytical HPLC on a dual pump Waters apparatus equipped with UV and radiation detectors. Analysis was performed using a Nova-Pak C18 column (3.9 x 150 mm) with a flow rate of 3 ml/min. Eluents components were A=0.1N TFA (trifluoroacetic acid) and B=CH_3CN (acetonitrile), and the following gradient elution technique was adopted for separation: 0-1.5 min 95% A + 5% B isocratic, 1.5-2.0 min from 5 to 100% B in linear gradient, 2-3 min 100% B, 3-4 min from 100 to 5% B in linear gradient.

HUMAN SUBJECTS

Five healthy subjects (mean age ± SD, 37.2 ± 15.6 y; age range, 28-65 y; 3 men and 2 women) were included. Prescreening consisted of a detailed medical history review and physical examination. Subjects with evidence of clinical disease or history of organ-removal surgery were excluded. The PET/CT scans were performed at the National Institute of Cancer under the approval of the Bioethical Committee. Written informed

consent was obtained from each subject. The subject´s weights were 79.2 ± 21.0 kg (range, 64-115 kg).

PET/CT ACQUISITION

Imaging was performed on a Biograph 16 PET/CT scanner (Siemens Medical Solutions, USA). To avid biological elimination, subjects urinated before the examination and did not urinate again until after the entire series of images was completed. Before administration of the tracer a low-dose CT scan without contrast was acquired for anatomic localization and attenuation correction. The helical CT scan acquisition parameters were 120 kVp, 180 mAs, and 5-mm slice thickness. After intravenous injection of ^{68}Ga-DOTA-E-[c(RGDfK)]$_2$ (198.3 ± 3.3 MBq), 3 consecutive whole-body (WB) emission scans were acquired approximately 30, 60, and 120 min after injection, in close agreement with a previous publication on the dosimetry of ^{68}Ga-DOTATATE in humans (33). The WB PET scans were acquired from the vertex to mid thighs, with 2-3 min per bed position in 3-dimensional mode. In order to keep the X-ray dose as low as possible, subjects remained motionless on the bed of the scanner until the entire series of emission scans was completed, so that the same CT scan can be used for the 3 emission scans. PET images were reconstructed using a 2-D ordered subset expectation maximization (OSEM 2D) algorithm, and were corrected for scatter, randoms, dead time, and decay. Resulting voxels were stored in units of Bq/ml.

IMAGING ANALYSIS

All PET/CT images were archived in Digital Imaging and Communications in Medicine (DICOM) format and were analyzed using OsiriX MD Imaging Software (Pixmeo SARL, Bernex, Switzerland). The source organs were chosen from visually identifiable regions of the PET/CT images, including the thyroid, spleen, liver, kidneys, urinary bladder, and the choroid plexus and ventricular system. Volumes of interest (VOIs) were drawn around the source organs and WB onto each frame of the 3 scans acquired. The total activity of each organ was determined multiplying the mean activity concentration (Bq/ml or Bq/cc) by the CT-derived

volume of interest, and the percentage of injected activity per organ (%IA/organ) was calculated as the ratio between the measured activity in the organ and activity in the WB of the scan acquired at the first time point (estimated to be about 80% because of omission of portions of the extremities). The activity expressed as percentage-injected dose was plotted against time to obtain the time-activity curves (TACs) of measured organs. The resulting TACs were fitted to exponential equations and the curves were extrapolated beyond the measured data points using the fitted equations.

RADIATION DOSIMETRY ESTIMATES

In this study, radiation absorbed doses and effective doses were calculated based on the RADAR method (34) by entering the normalized number of disintegrations of each source organ into OLINDA/EXM 1.1 software (Organ Level Internal Dose Assessment Code, Vanderbilt University, Nashville, USA), using the standardized adult male and female models (35). The OLINDA/EXM kinetic analysis module was used to calculate the normalized number of disintegrations (time-integrated activity coefficient) of organs showing an exponential decrease, such as thyroid, spleen, liver and kidneys. Organ volumes derived from CT were converted to mass using density values from the International Commission on Radiological Protection Publication 89 (ICRP-89). The normalized number of disintegrations in the urinary bladder wall was calculated using the OLINDA/EXM dynamic bladder model (36) with no voiding, and with a 1- and 2.5-h bladder voiding intervals. Finally, normalized number of disintegrations for the gastrointestinal tract were estimated using the the ICRP 30 gastrointestinal (GI) tract model included in the OLINDA/EXM code assuming an activity fraction of 0.05–0.07 entering to the small intestine, as images revealead that 6.0 ± 0.8% of the total activity was excreted into the intestine at 30 min p.i. This model assumes that a fraction of injected activity enters the small intestine with no reabsorption.

STATISTICAL METHODS

Data are presented as means ± SD unless otherwise stated.

RESULTS

The labeling yield was almost quantitative with a RCP >97% without the need of purification. The retention times for free $^{68}GaCl_3$ and ^{68}Ga-DOTA-E-[c(RGDfK)]$_2$ were 0.5 $\pm$ 0.1 and 2.5 $\pm$ 0.2 min, respectively. The content of the long-lived ^{68}Ge in the final product was <0.002% of the total radiactivity of ^{68}Ga, as measured by gamma spectroscopy using a HP-Germanium detector 48 h after the end of the radiolabeling synthesis.

The injection of 198.3 ± 3.3 MBq of ^{68}Ga-DOTA-E-[c(RGDfK)]$_2$ (17.7 ± 7.3 nmol of DOTA-E-[c(RGDfK)]$_2$) produced no observable adverse events or clinically detectable pharmacologic effects in any of the 5 subjects. Figure 2 shows representative normal biodistribution of the radiotracer at 30, 60, and 120 min after injection, while biodistribution data for the 5 subjects, expressed as percentage of injected activity per organ (%ID/organ), are shown in Table 1. TAC´s of the spleen, kidneys, liver and urinary bladder are shown in Fig. 3. The normalized number of disintegrations for the different organs in men and women are listed in Table 2, and the mean organ doses and effective doses are given in Table 3 for the different models used.

DISCUSSION

This study represents, to the best of our knowledge, the first in human biodistribution and radiation dosimetry measurements of a DOTA-conjugated dimeric RGD peptide labeled. The evaluated ^{68}Ga-DOTA-E-[c(RGDfK)]$_2$ revealed a biodistribution dominated by activity in the bladder, liver, kidneys, and spleen. The dosimetry calculations revealed the urinary bladder wall as the critical organ with a mean (all subjects, men and women) absorbed dose of 417 $\pm$ 71 μGy/MBq (mean $\pm$ SEM) for the kinetic input model (not voiding). This dose decreases to 360 $\pm$ 66 and 172 $\pm$ 31 μGy/MBq for the 2.5- and 1-h bladder-voiding models, respectively. On the other hand, the mean effective doses were 34.05 $\pm$ 4.85 μSv/MBq, 31.00 $\pm$ 2.37 μSv/MBq, and 20.85 $\pm$ 5.18 μSv/MBq (mean $\pm$ SEM) for the no bladder voiding, 2.5- and 1-h bladder-voiding models, respectively. Note that in general the radiation doses are higher for females than males; this is due to the smaller body and

organ sizes than those of her male counterpart. Additionally, female gonads are inside the body instead of outside, receiving a higher radiation dose given the proximity to several organs such as the urinary bladder, liver and kidneys, which are often important source organs. The small female sample size could be a limitation, but considering that for diagnostic purposes the most relevant is the effective dose, it is expected that the mean effective doses for most of the patients (all subjects, men and women) will be in the range reported in this study.

The radiation absorbed doses and effective doses of other RDG-based PET radiopharmaceuticals recently reported in the literature are listed in Table 4. This table shows that the effective dose of ^{68}Ga-DOTA-E-[c(RGDfK)]$_2$ is comparable to those of other ^{68}Ga- and ^{18}F-labeled radiopharmaceuticals. For a typical 185 MBq administered activity of ^{68}Ga-DOTA-E-[c(RGDfK)]$_2$, the effective dose for the 1-h bladder-voiding model is estimated to be 3.9 mSv, which is almost half of the estimated 7 mSv in a typical WB-PET scan with ^{18}F-FDG.

Of particular interest in this research was the observed uptake in the brain, specifically in the choroid plexus and ventricular system. Previous publications on biodistribution and radiation dosimetry of radiopharmaceuticals based on RGD-peptides do not mention such finding. However, other authors have reported the expression of a vast variety of integrin receptors in different structures of adult brain, including the heterodimeric $\alpha_V\beta_3$ and its subunits α_V and β_3, which may explain this uptake (37-39). Prediction of the partition coefficient for the Ga-RGD monomer is CLogP=-1.8651 and for Ga-RGD dimer is CLogP=-1.7783 (ChemBioDraw Ultra program). The small difference between these values not explains any possible ability of the dimer derivative to cross the blood brain barrier. Nevertheless, a clear choroid plexus visualization, as shown in Fig. 4, has not been previously reported in humans for any RGD radiopeptide and it could be associated with a higher in vivo affinity of the dimer molecule with respect to that of monomer, since integrins are significantly expressed in choroid plexus epithelial cells and microglia (40).

A clinical protocol to evaluate the potential of ^{68}Ga-DOTA-E-[c(RGDfK)]$_2$ as a predictive biomarker of outcome in non-small cell lung cancer in patients treated with combined Docetaxel and Nintedanib is currently in progress at the National Institute of Cancer.

CONCLUSION

We have successfully made measurements to estimate the ^{68}Ga-DOTA-E-[c(RGDfK)]$_2$ human dosimetry in 5 adult healthy subjects. These results provide the first, to the best of our knowledge, human dosimetry data of a DOTA-conjugated dimeric RGD peptide, and visualization of the choroid plexus and ventricular system with a radiopharmaceutical based in an RGD-peptide. The critical organ was urinary bladder wall with a mean absorbed dose of 172 $\pm$ 31 μGy/MBq for the 1-h bladder-voiding model. The mean effective dose, determined with the same model, was 20.85 $\pm$ 5.18 μSv/MBq. This radiopharmaceutical demonstrates a radiation dose comparable to other previously reported RGD-based radiopharmaceuticals labeled with ^{68}Ga and ^{18}F. In all cases, the urinary bladder wall had the highest dose among all the organs and is deemed to be the critical organ; however, with the use of diuretic agents and frequent bladder voiding doses to blabber wall and the WB can be reduced. Therefore, ^{68}Ga-DOTA-E-[c(RGDfK)]$_2$ can safely be used for imaging integrin $\alpha_V\beta_3$ expression.

ACKNOWLEDGMENTS

We thank the staff of Unidad Radiofarmacia-Ciclotrón, Efraín Zamora-Romo, Juan C. Manrique-Arias, Fernando Trejo-Ballado, Gabriela Contreras-Castañón, Héctor M. Gama-Romero, Adolfo Zárate-Morales, and Armando Flores-Moreno, for assistance in radiopharmaceutical production and quality control. We also thank the NM nurse Gildardo Gamez-Maldonado and the NMT José U. Martinez-Berry, Osvaldo Morales-Santillan and Mario E. Romero-Piña for their help in image acquisition. This research was supported by CONACYT Grant 179218, and International Atomic Energy Agency RC16467.

REFERENCES

1. Velikyan I. Molecular imaging and radiotherapy: theranostics for personalized patient management. *Theranostics*. 2012;2:424-426.
2. Fass L. Imaging and cancer: a review. *Mol Oncol*. 2008;2:115-152.
3. Chen K, and Conti PS. Target-specific delivery of peptide-based probes for PET imaging. *Adv Drug Deliv Rev*. 2010; 62:1005-1022.
4. Banerjee SR and Pomper MG. Clinical applications of Gallium-68. *Appl Radiat Isot*. 2013;76:2-13.
5. Kulkarni HR and Baum RP. Theranostics with Ga-68 somatostatin receptor PET/CT monitoring response to peptide receptor radionuclide therapy. *PET Clin*. 2014;9:91-97.
6. Kulkarni HR and Baum RP. Patient selection for personalized peptide receptor radionuclide therapy using Ga-68 somatostatin receptor PET/CT. *PET Clin*. 2014;9:83-90.
7. Haug AR, Auernhammer CJ, Wängler B, et al. ^{68}Ga-DOTATATE PET/CT for the early prediction of response to somatostatin receptor–mediated radionuclide therapy in patients with well-differentiated neuroendocrine tumors. *J Nucl Med*. 2010;51:1349-1356.
8. Walker RC, Smith GT, Liu E, et al. Measured human dosimetry of ^{68}Ga-DOTATATE. *J Nucl Med*. 2013;54:855-860.
9. Lopez-Rodriguez V, Gaspar-Carcamo RE, Pedraza-Lopez M, et al. Preparation and preclinical evaluation of ^{66}Ga-DOTA-E[c(RGDfK)]$_2$ as a new theranostic radiopharmaceutical. *Nucl Med Biol*. 2015;42:109-114.
10. Knetsch PA, Petrik M, Rangger C, et al. [^{68}Ga]NS3-RGD and [^{68}Ga] Oxo-DO3A-RGD for imaging $\alpha_v\beta_3$ integrin expression: synthesis, evaluation, and comparison. *Nucl Med Biol*. 2013;40:65–72.
11. Stott Reynolds TJ, Schehr R, Liu D, et al. Characterization and evaluation of DOTA-conjugated Bombesin/RGD-antagonists for prostate cancer tumor imaging and therapy. *Nucl Med Biol*. 2015;42:99-108.

12. Plow EF, Haas TA, Zhang L, et al. Ligand binding to Integrins. *J Biol Chem*. 2000;275:21785-21788.
13. Brooks PC. Role of integrins in angiogenesis. *Eur J Cancer*. 1996;32A:2423-2429.
14. Dijkgraaf I, Yim CB, Franssen GM, et al. PET imaging of $\alpha_V\beta_3$ integrin expression in tumours with ^{68}Ga-labelled mono, di- and tetrameric RGD peptides. *Eur J Nucl Mol Imaging*. 2011;38:128-137.
15. Decristoforo C, Hernandez Gonzalez I, Carlsen J, et al. ^{68}Ga- and ^{111}In-labelled DOTA RGD peptides for imaging of $\alpha_v\beta_3$ integrin expression. *Eur J Nucl Med Mol Imaging*. 2008;35:1507-1515.
16. Knetsch PA, Petrik M, Griessinger CM, et al. [^{68}Ga]NODAGA-RGD for imaging αvβ3 integrin expression. *Eur J Nucl Med Mol Imaging*. 2011;38:1303–1312.
17. Chen X, Tohme M, Park R, et al. Micro-PET imaging of alphavbeta3-integrin expression with 18F-labeled dimeric RGD peptide. *Mol Imaging*. 2004;3:96-104.
18. Ferro-Flores G, Ramírez F de M, Meléndez-Alafort L, et al. Peptides for In vivo target-specific cancer imaging. *Mini Rev Med Chem*. 2010;10:87-97.
19. Janssen M, Oyen WJ, Massuger LF, et al. Comparison of a monomeric and dimeric radiolabeled RGD-peptide for tumor targeting. *Cancer Biother Radiopharm*. 2002,17:641-646.
20. Liu S. Radiolabeled multimeric cyclic RGD peptides as integrin $\alpha_v\beta_3$ targeted radiotracers for tumor imaging. *Mol Pharm*. 2006;3:472-487.
21. Li ZB, Chen k, Chen X. 68Ga-labeled multimeric RGD peptides for microPET imaging of integrin $\alpha_V\beta_3$ expression. *Eur J Nucl Med Mol Imaging*. 2008;35:1100-1108.
22. Fani M, Andre JP and Maecke HR. 68Ga-PET: a powerful generator-based alternative to cyclotron-based PET radiopharmaceuticals. *Contrast Media Mol Imaging*. 2008;3:53-63.
23. Rösch F and Baum RP. Generator-based PET radiopharmaceuticals for molecular imaging of tumours: on the way to Theranostics. *Dalton Trans*. 2011;40:6104-6111.
24. Rösch F. Past, present and future of ^{68}Ge/^{68}Ga generators. *Appl Radiat Isot*. 2013;76:24-30.

25. Decristoforo C, Pickett RD, Verbruggen A. Feasibility and availability of ^{68}Ga-labelled peptides. *Eur J Nucl Med Mol Imaging*. 2012;39:31-40.
26. Beer AJ, Haubner R, Wolf I, et al. PET-based human dosimetry of 18F-galacto-RGD, a new radiotracer for imaging alpha$_V$beta$_3$ expression. *J Nucl Med*. 2006;47:763-769.
27. Doss M, Kolb HC, Zhang JJ, et al. Biodistribution and radiation dosimetry of the integrin marker ^{18}F-RGD-K5 determined from whole-body PET/CT in monkeys and humans. *J Nucl Med*. 2012;53:787-795.
28. Kim JH, Lee JS, Kang KW, et al. Whole-body distribution and radiation dosimetry of 68Ga-NOTA-RGD, a positron emission tomography agent for angiogenesis imaging. *Cancer Biother Radiopharm*. 2012;27:65-71.
29. Chen X, Liu S, Hou Y, et al. MicroPET imaging of breast cancer alphav-integrin expression with ^{64}Cu-labeled dimeric RGD peptides. *Mol Imaging Biol*. 2004;6:350-359.
30. Janssen ML, Oyen WJ, Dijkgraaf I, et al. Tumor targeting with radiolabeled $\alpha_v\beta_3$ integrin binding peptides in a nude mouse model. *Cancer Res*. 2002;62:6146-6151.
31. Ortiz-Arzate Z, Santos-Cuevas CL, Ocampo-García BE, et al. Kit preparation and biokinetics in women of ^{99m}Tc-EDDA/HYNIC-E-[c(RGDfK)]$_2$ for breast cancer imaging. *Nucl Med Commun*. 2014;35:423-432.
32. Ma Q, Ji B, Jia B, et al. Differential diagnosis of solitary pulmonary nodules using ^{99m}Tc-3P4-RGD$_2$ scintigraphy. *Eur J Nucl Med Mol Imaging*. 2011;38:2145–2152.
33. Walker RC, Smith GT, Liu E, Moore B, Clanton J, Stabin M. Measured Human Dosimetry of ^{68}Ga-DOTATATE. J Nucl Med. 2013;54:855-860.
34. Stabin MG and Siegel JA. Physical Models and Dose Factors for Use in Internal Dose Assessment. *Health Phys*. 2003; 85:294-310.
35. Stabin MG, Sparks RB, Crowe E. OLINDA/EXM: The second-generation personal computer software for internal dose assessment in nuclear medicine. *J Nucl Med*. 2005;46:1023–1027.
36. Thomas SR, Stabin MG, Chen CT, Samaratunga RC. MIRD Pamphlet No. 14 revised: A dynamic urinary bladder model for radiation dose calculations. Task Group of the MIRD Committee, Society of Nuclear Medicine. *J Nucl Med*. 1999;40:102S-123S.

37. Paulus W, Baur I, Schuppan D, et al. Characterization of integrin receptors in normal and neoplastic human brain. *Am J Pathol*. 1993;143:154-163.
38. Pinkstaff JK, Detterich J, Lynch G, et al. Integrin subunit gene expression is regionally differentiated in adult brain. *J Neurosci*. 1999;19:1541–1556.
39. Wu X and Reddy DS. Integrins as receptor targets for neurological disorders. *J Pharmacol Ther*. 2012;134:68–81.
40. Engelhardt B, Sorokin L. The blood-brain and the blood-cerebrospinal fluid barriers: function and dysfunction. *Semin Immunopathol*. 2009;31:497-511.

Figure 1

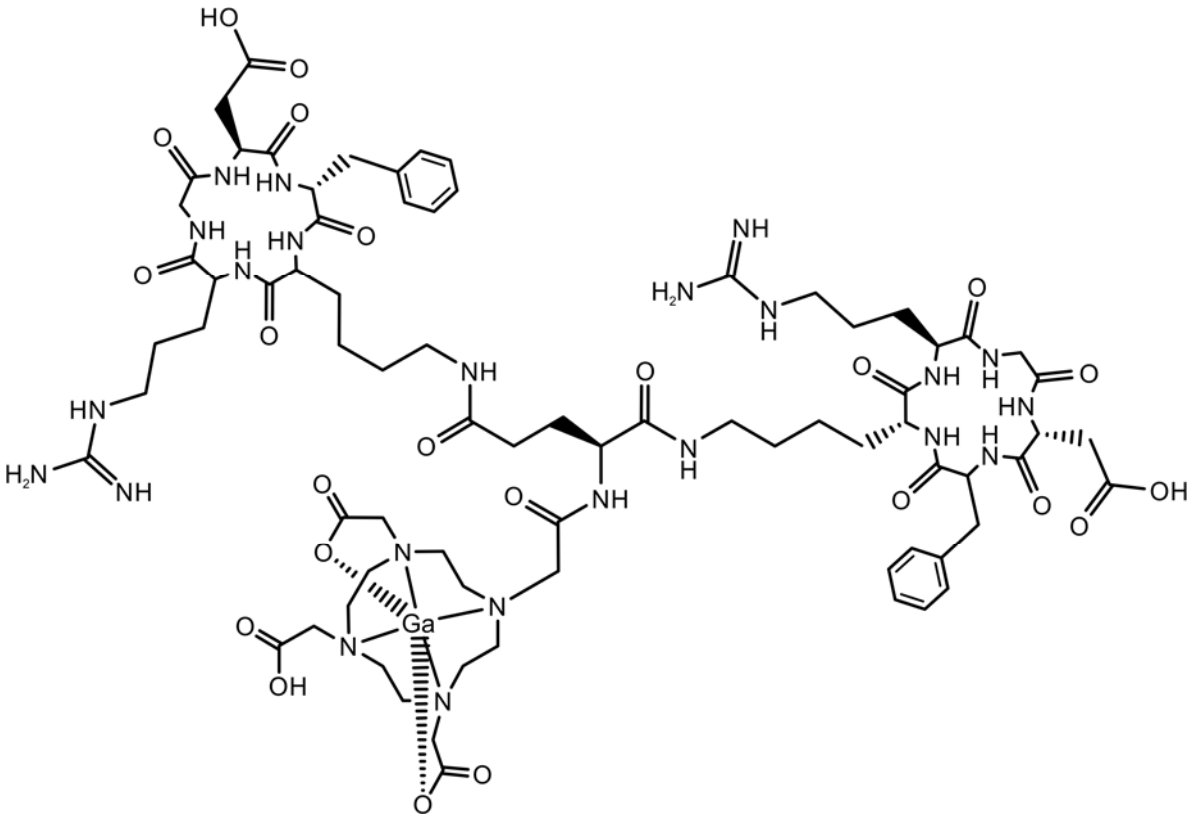

FIGURE 1. Estructural formula of ^{68}Ga-DOTA-E-[c(RGDfK)]$_2$

Figure 2

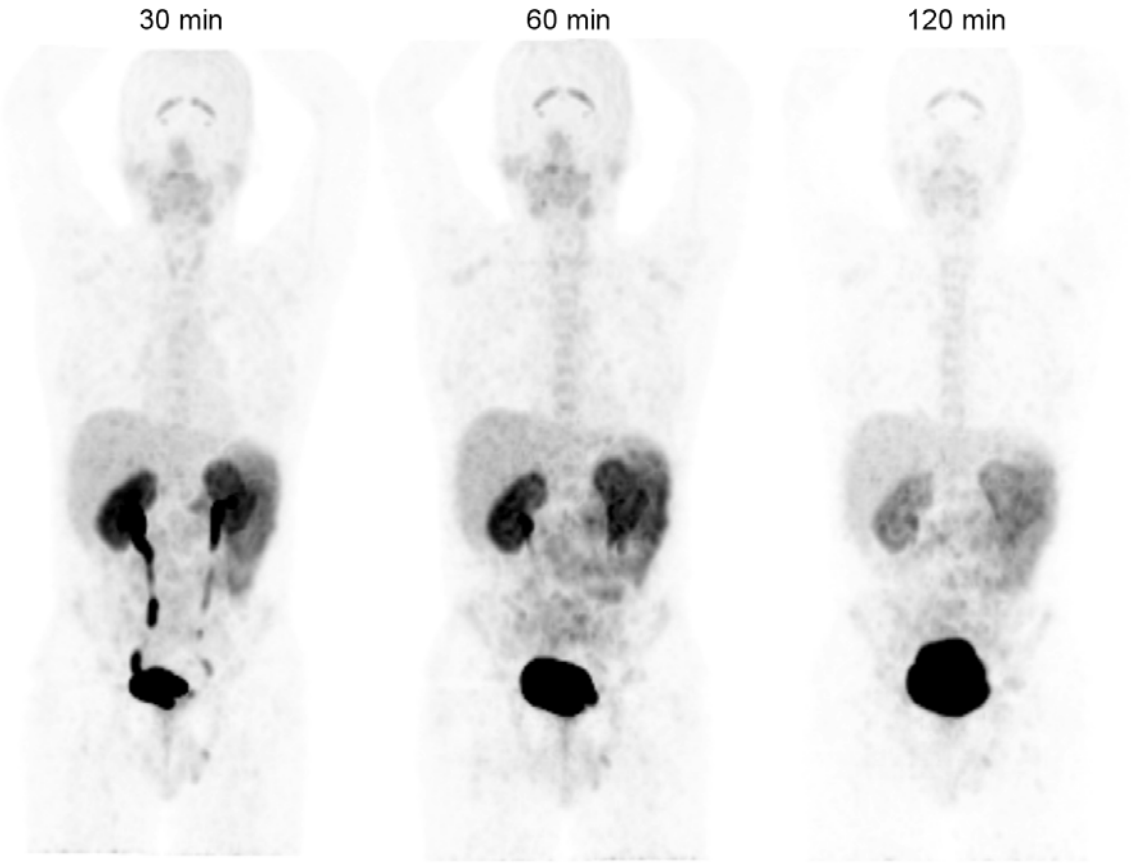

FIGURE 2. Typical normal biodistribution of ^{68}Ga-DOTA-E-[c(RGDfK)]$_2$ at 30, 60, and 120 min after injection.

Figure 3

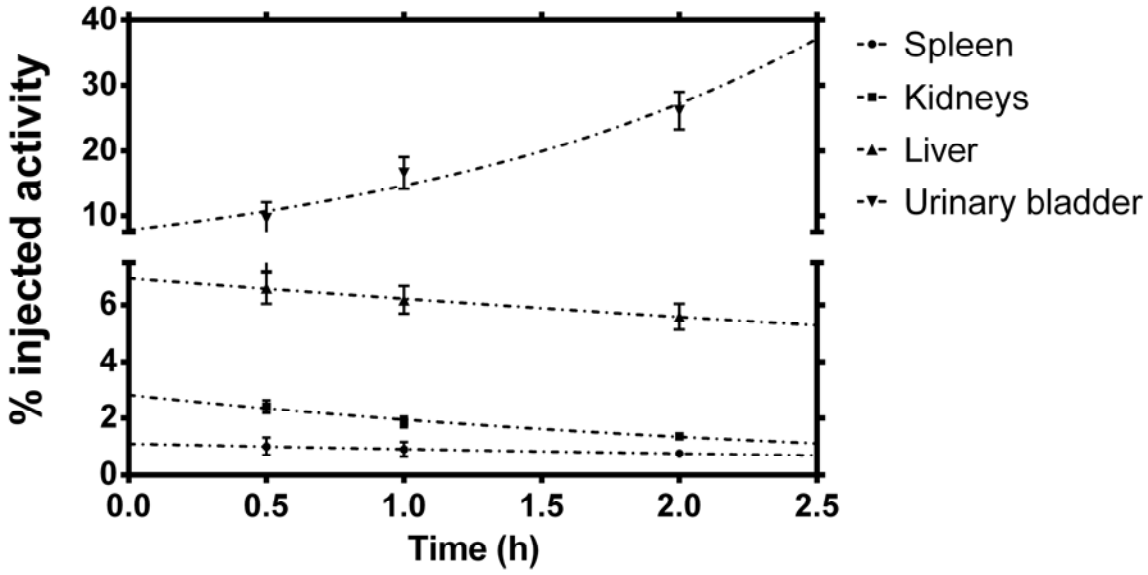

FIGURE 3. Time activity curves (TACs) of the spleen, kidneys, liver and urinary bladder.

Figure 4

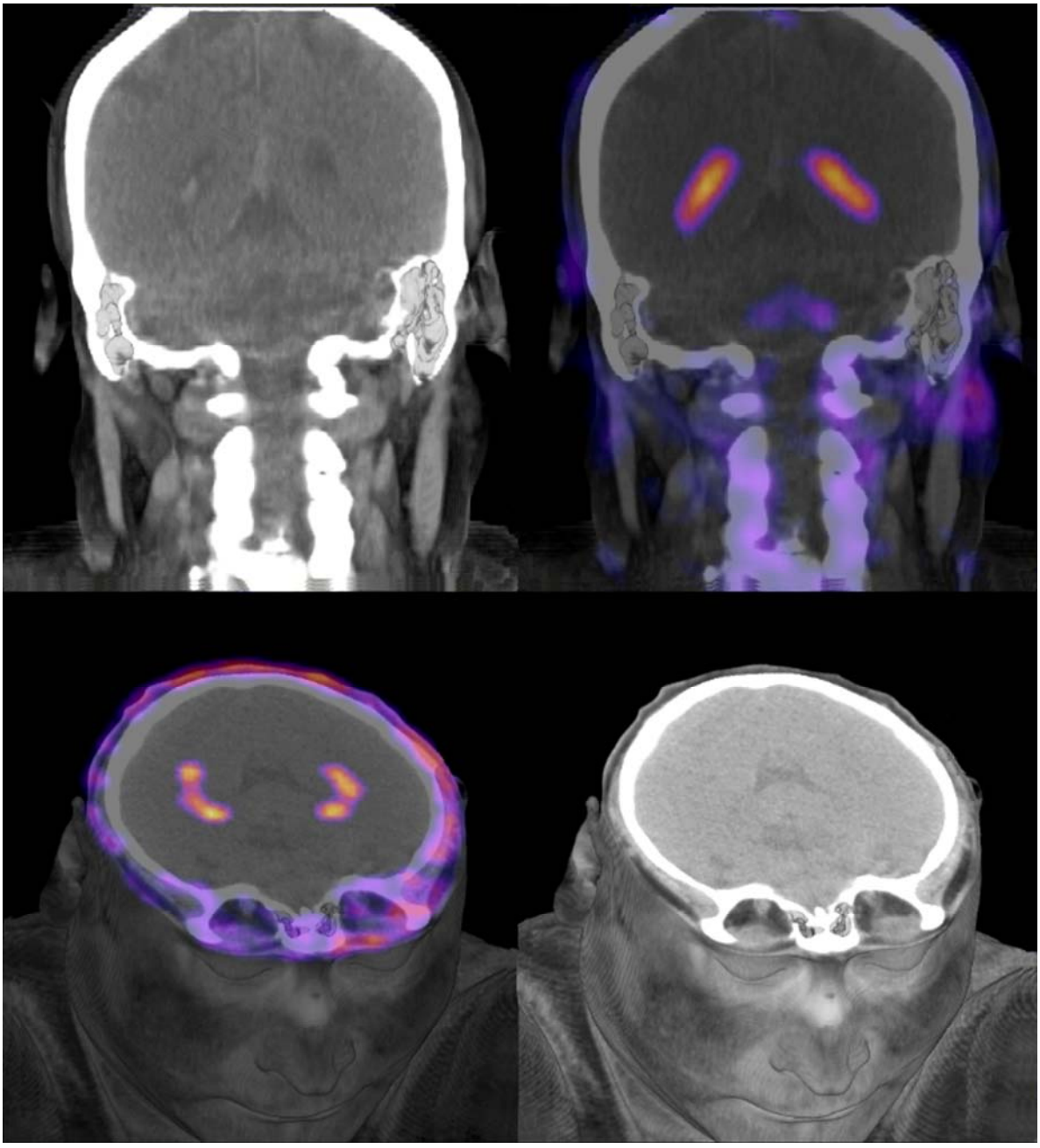

FIGURE 4. PET/CT and CT images showing the normal uptake of ^{68}Ga-DOTA-E-[c(RGDfK)]$_2$ in choroids plexus at the supratentorial ventricular system.

TABLE 1. Biodistribution in healthy subjects after intravenous administration of ^{68}Ga-DOTA-E-[c(RGDfK)]$_2$, expressed as a percentage of the injected dose per organ (%ID/organ) (mean ± SD).

Tissue	0.5 h	1 h	2 h
Choroid plexus	0.0393 ±0.0018	0.0350±0.0014	0.0266±0.0030
Thyroid	0.0504±0.0051	0.0447±0.0047	0.0342±0.0015
Spleen	1.0058±0.1374	0.9020±0.1128	0.7578±0.0615
Kidneys	2.4065±0.2234	1.8632±0.1883	1.3657±0.0677
Liver	6.594±0.5563	6.1797±0.4814	5.5931±0.4498
Urinary bladder	9.6152±2.4242	16.5708±2.4702	26.1134±2.8535

TABLE 2. Number of disintegrations of source organs (mean ± SD) for healthy subjects injected with ^{68}Ga-DOTA-E-[c(RGDfK)]$_2$

Source organ	Male (MBq·h/MBq, n=3)	Female (MBq·h/MBq, n=2)
Choroid plexus	5.43E-04±7.51E-05	5.50E-04±1.00E-05
Lower large intestine wall	2.97E-03±7.02E-04	3.60E-03±2.83E-04
Small Intestine	7.05E-02±1.63E-02	8.49E-02±6.93E-03
Upper large intestine wall	2.54E-02±5.88E-03	3.07E-02±2.55E-03
Kidneys	3.28E-02±6.26E-03	3.30E-02±1.41E-02
Liver	8.95E-02±1.78E-02	1.16E-01±5.66E-03
Spleen	1.43E-02±3.77E-03	1.41E-02±3.82E-03
Thyroid	6.93E-04±6.35E-05	6.70E-04±1.56E-04
Urinary Bladder Contents (no voiding)	3.10E-01±1.22E-01	2.98E-01±1.11E-01
Urinary Bladder Contents (1-h voiding)	1.12E-01±4.44E-02	1.27E-01±6.04E-02
Urinary Bladder Contents (2.5-h voiding)	2.42E-01±9.36E-02	2.74E-01±9.10E-02
Remainder	8.09E-01±1.08E-01	7.89E-01±1.34E-01

TABLE 3. Absorbed radiation doses and the effective doses (mean ± SEM) of ^{68}Ga-DOTA-E-[c(RGDfK)]$_2$ in healthy subjects using different urinary bladder models.

Target organ	Male (μGy/MBq, n=3)			Female (μGy/MBq, n=2)		
	No voiding	1 h BVM	2.5 h BVM	No voiding	1 h BVM	2.5 h BVM
Adrenals	9.2±0.6	9.1±0.6	9.2±0.6	12.0±0.8	11.9±0.8	12.0±0.8
Brain	6.5±0.5	6.5±0.5	6.5±0.5	8.2±0.7	8.2±0.7	8.2±0.7
Breasts	6.6±0.5	6.6±0.5	6.6±0.5	8.4±0.9	8.4±0.9	8.4±0.9
Gallbladder Wall	10.8±0.7	10.7±0.8	10.8±0.8	14.1±0.8	13.9±0.9	14.1±0.8
Lower large intestine wall	17.3±0.6	14.7±1.2	16.4±1.3	22.0±0.7	19.2±0.1	21.6±0.9
Small Intestine	47.5±5.2	46.5±5.4	47.2±5.3	64.3±2.6	63.1±2.4	64.1±2.7
Stomach Wall	8.9±0.6	8.7±0.6	8.8±0.6	11.2±0.9	11.1±0.9	11.2±0.9
Upper large intestine wall	36.2±3.8	35.5±3.9	36.0±3.9	48.3±1.6	47.4±1.4	48.2±1.7
Heart Wall	8.0±0.6	8.0±0.6	8.0±0.6	10.3±1.1	10.3±1.1	10.3±1.1
Kidneys	53.9±5.4	53.8±5.3	53.9±5.3	59.6±16.5	59.4±16.4	59.6±16.5
Liver	26.6±2.9	26.5±2.9	26.5±2.9	45.1±1.6	45.0±1.6	45.1±1.6
Lungs	7.5±0.6	7.5±0.6	7.5±0.6	9.7±1.0	9.7±1.0	9.7±1.0
Muscle	8.4±0.3	7.8±0.6	8.2±0.6	10.5±0.6	9.8±0.8	10.4±0.6
Ovaries*	13.5±0.2	11.1±0.8	12.7±1.0	17.3±0.4	14.6±0.3	17.0±0.6
Pancreas	9.6±0.6	9.5±0.6	9.6±0.6	12.2±0.8	12.2±0.9	12.2±0.8
Red Marrow	7.1±0.3	6.7±0.5	7.0±0.5	8.8±0.5	8.3±0.6	8.7±0.5
Osteogenic Cells	10.7±0.7	10.4±0.8	10.6±0.8	14.3±1.4	14.1±1.5	14.3±1.4
Skin	6.7±0.4	6.5±0.5	6.7±0.5	8.4±0.8	8.1±0.8	8.3±0.8
Spleen	39.2±5.5	39.1±5.5	39.1±5.5	47.1±8.2	47.0±8.2	47.1±8.2
Testes	9.7±0.1	8.0±0.7	9.1±0.8	0.0±0.0	0.0±0.0	0.0±0.0
Thymus	7.3±0.6	7.3±0.6	7.3±0.6	9.3±1.0	9.3±1.1	9.3±1.1
Thyroid	16.5±0.6	16.5±0.6	16.5±0.6	19.1±2.5	19.1±2.5	19.1±2.5
Urinary Bladder Wall	363±80	136±30	285±62	471±121	206±66	435±140
Uterus*	18.1±1.3	12.5±1.1	16.2±1.7	21.7±1.7	16.1±0.5	20.9±2.0
Total Body	9.8±0.4	9.1±0.7	9.6±0.7	12.6±0.5	11.9±0.7	12.6±0.5
Effective Dose (μSv/MBq)	29.6±3.7	17.4±1.7	25.4±3.3	38.5±6.0	24.3±3.1	36.6±7.1

*Dosimetric calculations for men, BVM: Bladder-voiding model.

TABLE 4. Comparison of radiation absorbed dose to critical organ and effective dose (mean ± SD) for different RGD-based radiopharmaceuticals (1-h bladder voiding model).

	^{18}F-Galacto-RGD (Ref 26)	^{18}F-RGD-K5 (Ref 27)	^{68}Ga-NOTA-RGD (Ref 28)	^{68}Ga-DOTA-RGD$_2$ (This work)
Urinary bladder wall (μGy/MBq)	110±20	103±4	208.60±50.79	172±100
Effective dose (μSv/MBq)	12.7±2.2	15.1±1	23.32±4.16	20.85±5.07
Typical injected activity (MBq)	370	370	185	185
Estimated ED per scan (mSv)	4.7	5.6	4.3	3.9